FLOW SEPARATION PREDICTION ON INLETS WITH MACH & REYNOLDS NUMBER EFFECTS IN SUBSONIC FLIGHT

Dr. R. K. Nangia, Dr M. E. Palmer
Consulting Engineers,
Nangia Aero Research Associates,
Maggs House, Queens Road,
Bristol, BS8 1QX, UK
Tel: +44 (117)-907 5595 Fax: +44 (117)-921 1594

Mr. J. Hodges
High Speed & Weapons Aerodynamics Dept.,
Aircraft Sector,
Defence Research Agency,
Bedford, MK41 6AE, UK
Tel: +44 (0)123-422 5009 Fax: +44 (0)123-422 5848

SUMMARY

Different types of inlets (cowls) are in use and the choice depends upon operational and configuration layout restraints. For various reasons, combat aircraft require engines to be set close to the fuselage centre-line. Further compromises may occur due to stealth, supersonic, transonic and low-speed capability and installation effects. In civil aircraft, performance, safety, passenger comfort and maintenance considerations lead to "isolated" engine pods. Such inlets are characterised by the need for good transonic design. In both cases, Mass Flow Ratio (MFR) requirements at incidence can be challenging, for example in take-off, landing or manoeuvring situations.

For a given inlet, the onset of external or internal flow separation limits the flight envelope. External separation causes a drag increase and internal separation causes distortions at the engine face. The ability to predict the onset of flow separations is therefore important for their prevention.

This paper describes the evaluation and correlation of a predictive method for the onset of flow separation. Axi-symmetric circular inlets with and without α effects are considered first. Encouraging correlation between theory and experiment leads to the extension of the methodology to 3-D inlets. The technique addresses the effects of Mach and Reynolds number on inlets in a general way and compared with other approaches available, the capabilities are more design related.

The method has the potential of providing encouraging cost and time savings. New project configurations can be evaluated at an early design stage with allowance for scale effects. Configuration layout and flight envelope can all be considered. Optimisation and parametric studies can be carried out using the theory prior to conventional, costly experimental programmes (wind tunnel and full-scale). The theory can also be used to define key areas (M, R, α, ß and MFR) that need to be carefully assessed at the test / evaluation stage.

1. INTRODUCTION

The choice of an engine inlet (**Fig.1**, Ref.1) depends upon operational and configuration layout restraints.

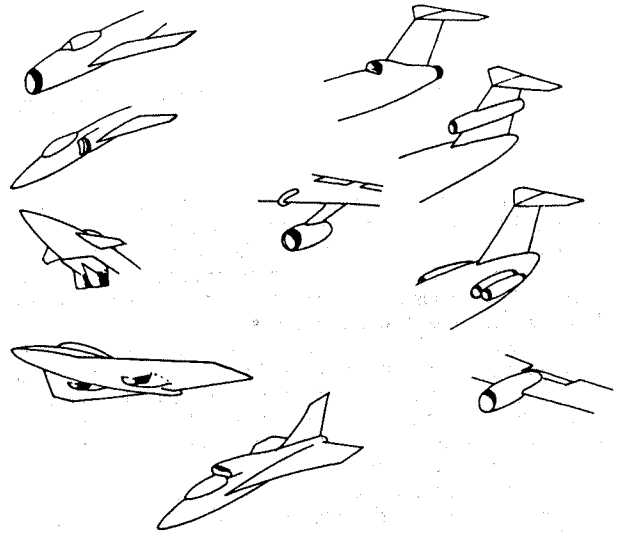

FIG. 1 TYPICAL INLET CONFIGURATIONS & LAYOUTS

For various reasons, combat aircraft require engines to be set close to the fuselage centre-line, Ref.2. Further compromises occur because of other considerations e.g. stealth (angled surfaces), supersonic capability (thin lips), transonic and low-speed agility (thicker lips) and installation (flow-fields with high tolerance to aircraft incidence α and side-slip ß). The Mass Flow Ratio (MFR) requirements can be challenging particularly in manoeuvring situations.

For civil aircraft, performance, safety, passenger comfort and maintenance considerations lead to "isolated" engine pods or a tail location, Ref.2. Such inlets are characterised by the need for good transonic design (low distortions) with high MFR capability at low forward velocities (take-off rotation). The incidence effects can be very strong for isolated inlets and although side-slip effects are present, these are not extreme.

For a given inlet, the flight envelope implies 3-D design for wide ranges of Mach number (M), Reynolds number (R), MFR, α and ß capabilities, Refs.3 and 4. The onset of external or internal flow separation, limits the flight envelope (**Fig.2**). External separation causes a drag increase and internal

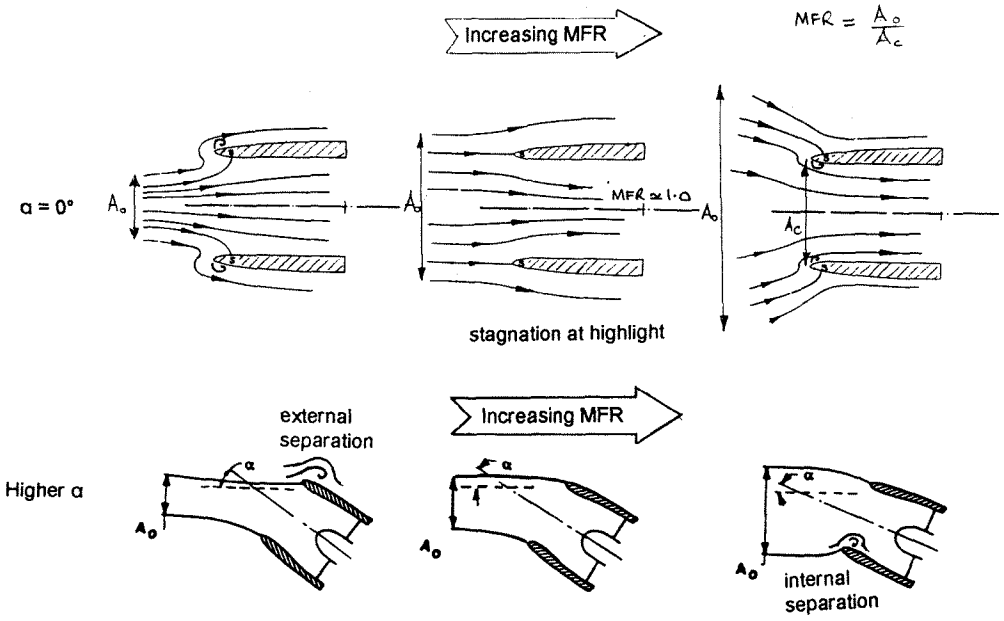

FIG. 2 EFFECT OF MFR & α , ONSET OF EXTERNAL & INTERNAL LIP SEPARATION

separations cause distortions at the engine face, leading eventually to compressor surge and possible structural damage, Refs.2 and 4. The ability to predict the onset of flow separations is therefore important for their prevention and also to enable more optimum design with shorter ducts. The knowledge also leads to "focussed" test programmes.

The order of complexity of inlet design and analysis from axisymmetric to stealthy types is shown in **Fig.3**. The "critical" areas (high suctions) tend to re-distribute themselves around the inlet face, with changing geometry and flow environment (M, R, α and ß). Hence for the raked/scarfed inlet, the "critical" area is the forward-swept corner as indicated.

Conventionally, the prediction of inlet flows has mainly evolved from an experimental basis (wind tunnel or full-scale) and high costs and time factors are implicit. The current project scene is more "paced" and emphasises cost and time reductions. It is prudent therefore to seek theoretical / empirical techniques.

This paper focusses first on the prediction and evaluation methodology for flow separation onset on axi-symmetric circular inlets with and without α effects. The approach is then extended to 3-D prismatic inlets.

2. PREDICTION TECHNIQUE

The technique developed addresses the effects of Mach number and Reynolds number on the LE thrust characteristics of inlets in a general way. Compared with other approaches available, the capabilities are more design related as regimes of attached flow (full 100% LE suction) and separated flow (< 100% LE suction) can be differentiated (onset of flow separations). The main principle is that increasing Reynolds number at a given Mach number permits a higher proportion of thrust levels to be "attained". On the other hand, increasing Mach number at a given Reynolds number, reduces the LE suction level attained (**Fig.4**). Thin (or sharper) lips reduce the attained thrust levels.

Semi-empirical correlations of LE suction attainment factors have been derived from several studies on wings and aerofoils and the relationships obtained have been incorporated in a cost-effective approach on desk-top computers. The

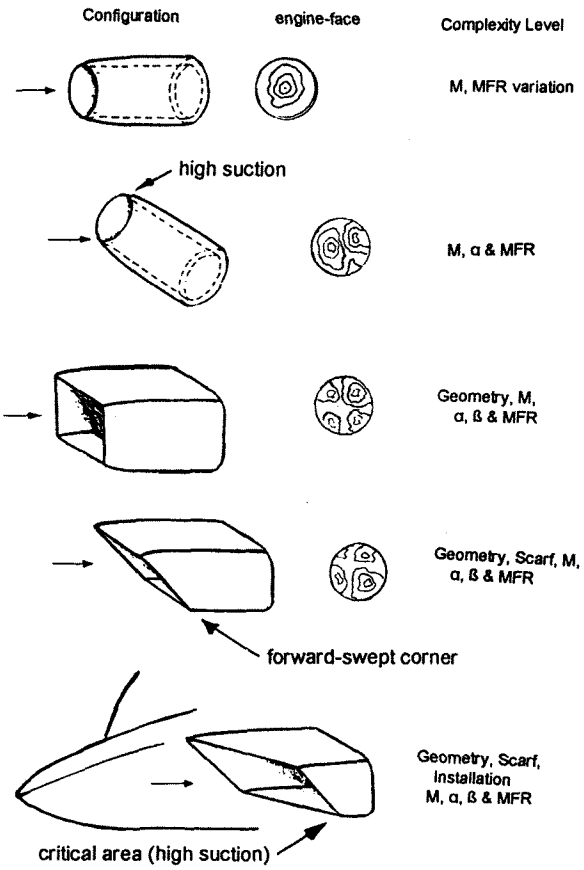

FIG. 3 ORDER OF COMPLEXITY, INLET DESIGN

method requires, as input, various geometry parameters and the cowl-lip thrust - MFR relationships. The latter can be evaluated by suitable flow solvers. In general, sub-critical panel methods have been found to be adequate for subsonic applications. Full potential solvers are applicable to certain transonic and mildly supersonic flows. The Euler prediction solvers should be applicable to general transonic and supersonic flows, Ref. 5.

Most of the work presented in this paper has been developed with sub-critical panel methods; an obvious advantage being that, the inlet lip (LE) pressures can be calculated to the desired accuracy without a field-grid. Thus complex 3-D geometries can be generated and run without large cpu requirements. On the downside, of course, is that compressibility effects are not tackled beyond the usual applicability of the Prandtl-Glauert scaling laws (say $M < 0.8$).

3. AXI-SYMMETRIC INLETS AT INCIDENCE

We focus on the axi-symmetric circular inlets to show some experimental results and assess the capabilites of the prediction and evaluation methodology for flow separation onset with and without incidence effects.

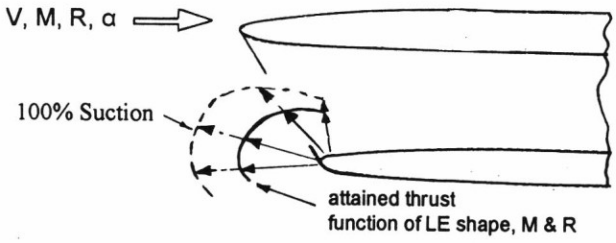

FIG. 4 ATTAINED THRUST PRINCIPLES, INLETS

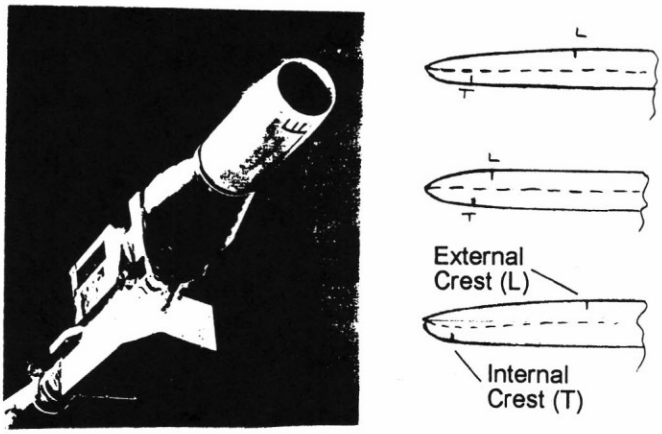

FIG. 5 MODEL IN WIND TUNNEL

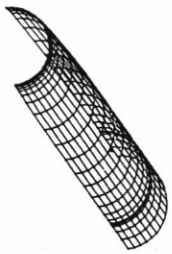

FIG. 6 THEORETICAL PANELLING, AXISYMMETRIC INLET

3.1. Geometry, Test Programme & Results

In a test programme dedicated to the study of flow separation onset, a series of axi-symmetric circular inlets were tested at incidence in the DRA 8ft wind tunnel, at Mach 0.45, 0.6 and 0.8, at two values of tunnel total pressure (H_0 = 32" Hg and 60" Hg). Varying H_0 gave two values of Reynolds number, R_1 (low) and R_2 (high). Reynolds number values quoted are based on a reference length equal to the model diameter (D). Results from a separate (earlier) series of tests (Reynolds number similar to R_1) have also been used for comparative purposes. A typical model is shown in **Fig.5** together with sketches of the various lip geometries. Internal and external crest locations were varied producing inward or outward camber and changes in contraction ratio. See also Ref.3.

Fig.6 shows a typical numerical panel representation. Using such geometry, the first important role of the theory was to derive the MFR test range for given Mach and Reynolds number combinations that encompassed the onset of flow separation closely. The wind tunnel role then became largely confirmatory. This in turn enabled several extra inlets to be tested during the wind tunnel occupancy period. The test arrangement did not feature ejectors to enable measurements at high values of MFR. This implied typically obtainable MFR ranges, in the tests, of up to 0.81 at Mach 0.45 and up to 0.87 at Mach 0.8.

Here we shall restrict the presentation to results of two inlets denoted simply as Inlet-A and Inlet-B. These are compared in **Fig.7** and have the following geometry definition:

INLET	CR	A_c/A_{max}
A	1.177	0.729
B	1.250	0.797

The external LE profiles are defined by a NACA-1 section and the internal profiles are elliptic with a/b ratios of 5. Consequently, the internal and external lip radii (r_{int} and r_{ext}) are different. Inlet-B has the higher contraction ratio afforded by a larger highlight diameter whilst retaining the same internal throat diameter. Inlet-A therefore has more inward camber than Inlet-B. The external crests are at similar streamwise locations. The internal crest of Inlet-A is noticeably farther forward than that of Inlet-B.

3.2. Results on Inlet-A

Fig.8 compares surface static pressures along a streamwise section of the inlet lip, theory and experiment (earlier tests, low Reynolds number), at Mach 0.6, $\alpha = 0.0°$, over the range $0.40 < MFR < 0.64$. External pressure distributions at $MFR > 0.64$ compared well but as MFR was reduced, flow separation occurred at about MFR = 0.65. At MFR = 0.641, experiment gives an indication of flow separation (discontinuity in pressures as marked). At MFR = 0.588, the results from experiment indicate a reduced peak suction ($C_{P\,min}$) and a modified pressure distribution due to separation. Internal pressure distributions compare well over this MFR range, even at conditions where external separation exists. Aft of the throat, the internal pressures are slightly different due to the wind tunnel model having a slightly divergent duct and the theoretical model having a parallel duct.

Fig.9 shows pressures from experiment at the lower centre-line station ($\phi = 180°$) at Mach 0.6, $\alpha = 10.0°$ and $0.27 < MFR < 0.87$. At incidence, the asymmetry implies a 3-D flow-field. The lower lip is more critical from the point of view of internal separation, whereas the upper lip is susceptible to external separation as MFR is reduced. In this case, the lower lip, there are no indications of internal flow separation and external flow separation is delayed until MFR = 0.3 (c.f. MFR = 0.6 at $\alpha = 0.0°$)

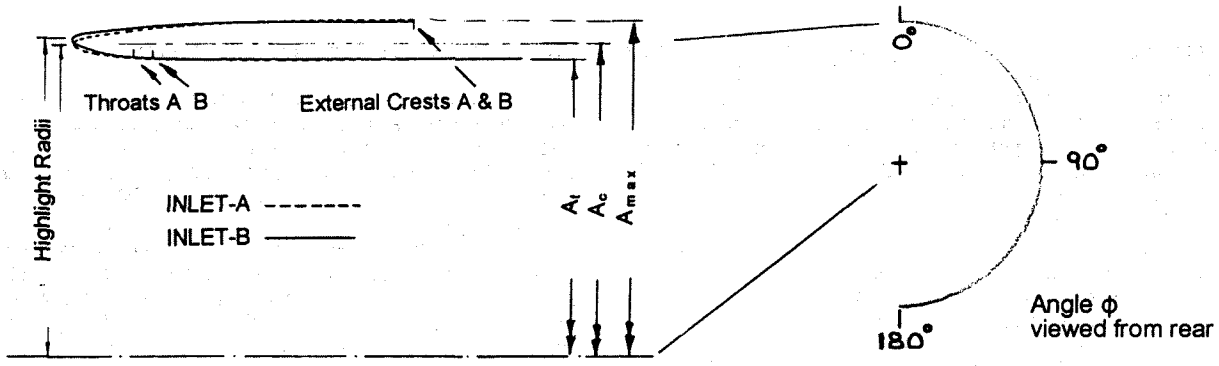

FIG. 7 COMPARISON OF INLET-A & INLET-B GEOMETRY

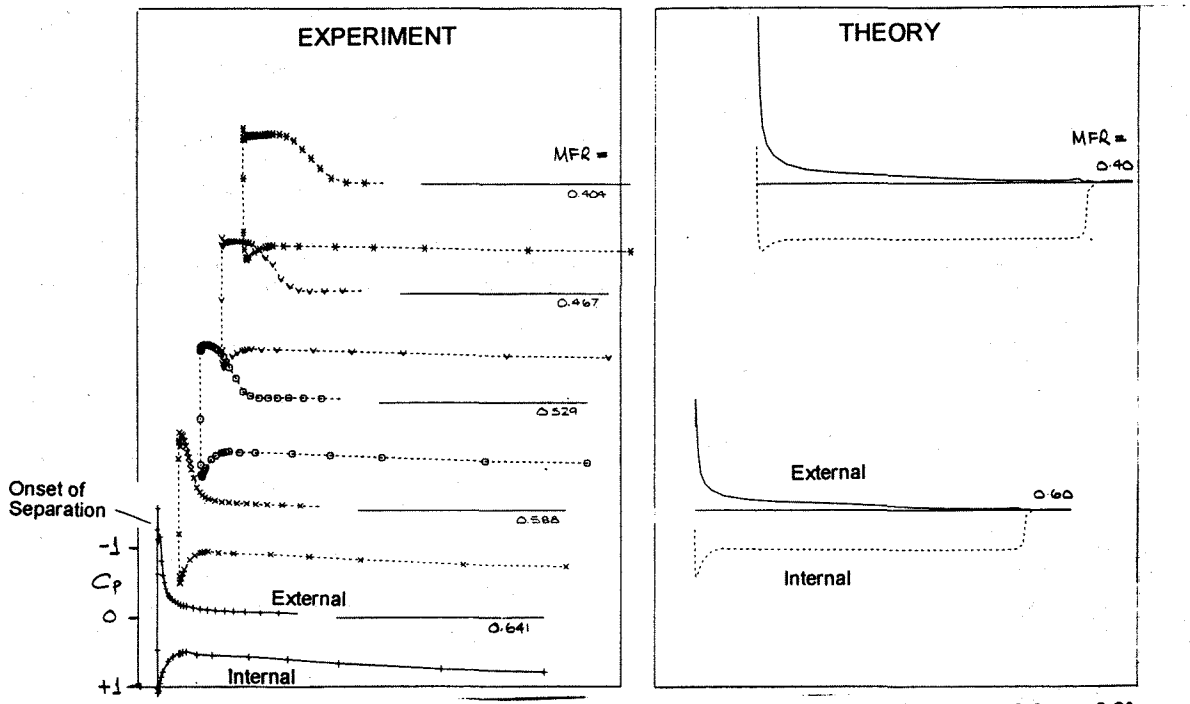

FIG. 8 INLET-A, THEORY & EXPERIMENTAL PRESSURES, EFFECT OF MFR, Mach 0.6, α = 0.0°

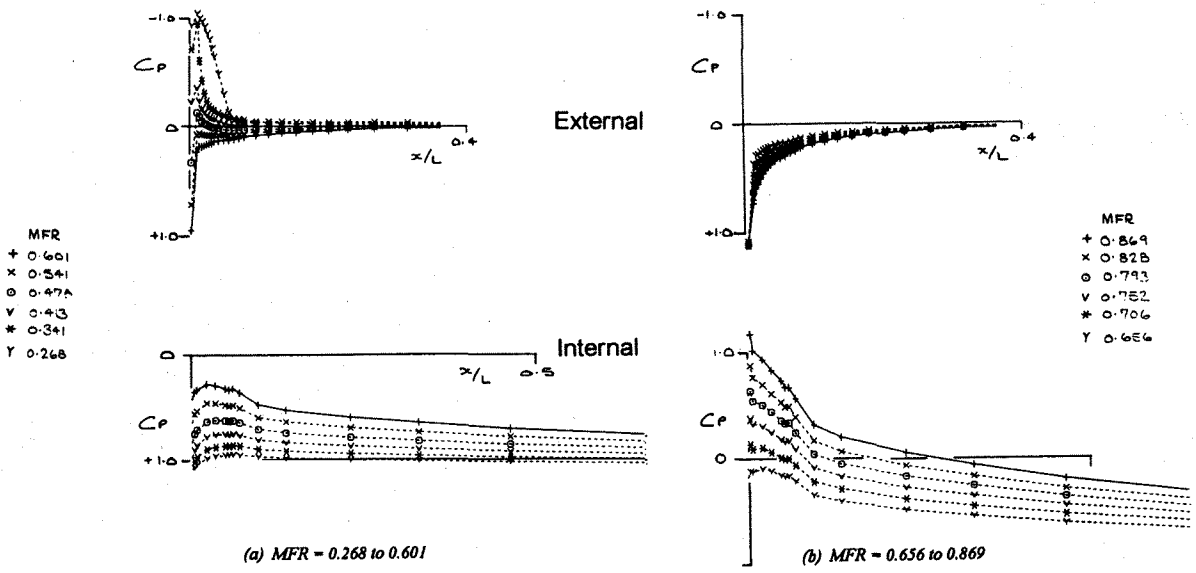

FIG. 9 INLET-A, EXPERIMENTAL PRESSURES ON INLET LOWER CENTRE-LINE, EFFECT OF MFR, Mach 0.6, α = 10°

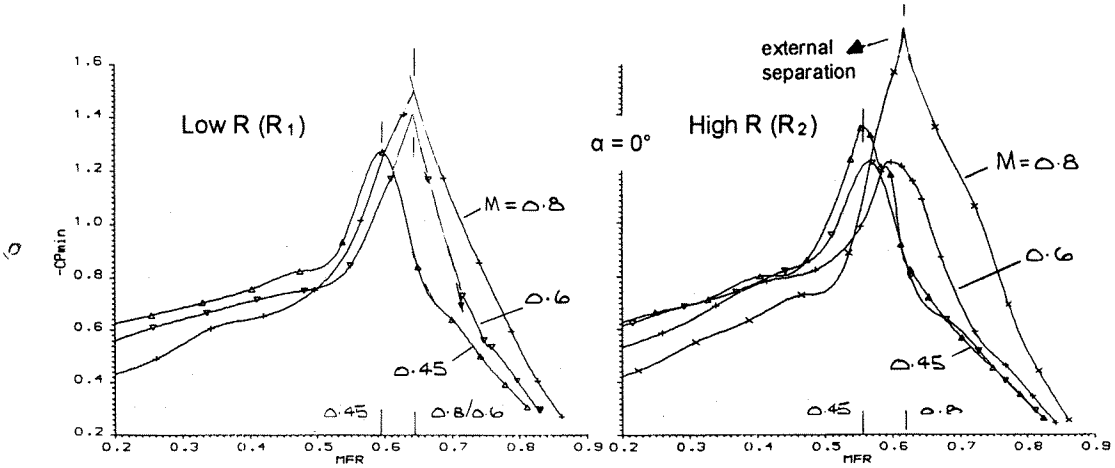

FIG. 10 INLET-A, EXPERIMENTAL C_P TO DISPLAY ONSET OF EXTERNAL FLOW SEPARATION, α = 0°, Mach 0.45, 0.6 & 0.8, R = 1.0 & 1.7 x10^6

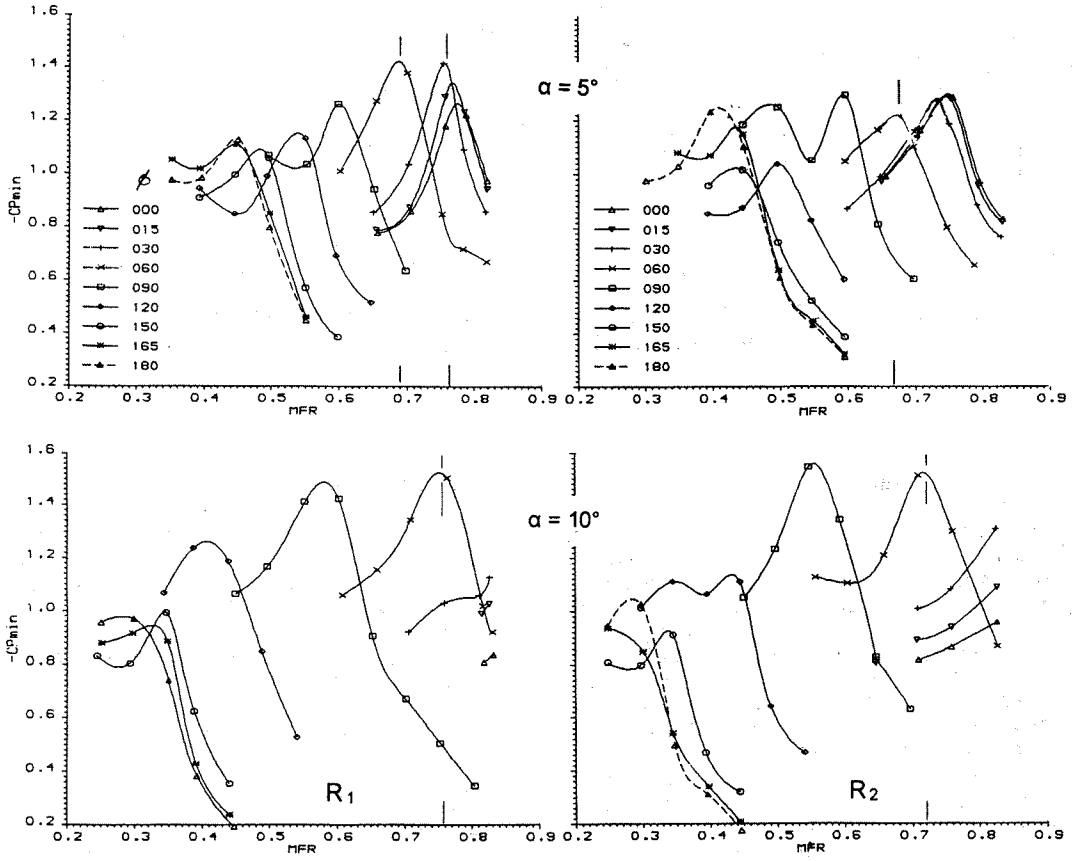

FIG. 11 INLET-A, EXPERIMENTAL C_P TO DISPLAY ONSET OF EXTERNAL FLOW SEPARATION, α = 5° & 10°, Mach 0.45, R = 1.0 & 1.7 x10^6

Flow Separation Onset Boundaries, Comparisons

Fig.10 shows plots of C_{Pmin} near the LE from experiment at α = 0.0°, Mach 0.45, 0.6 and 0.8, at low and high Reynolds numbers (R_1 & R_2). The onset of flow separation can be determined from the discontinuity in the C_{Pmin} curve as MFR is reduced. As Mach number is increased, separation occurs at higher MFR. The effect of increasing R is to delay the onset of flow separation. The effects of incidence on the separation distribution around the inlet lip are shown in **Fig.11** (α = 5.0° and 10.0°, Mach 0.45). The effects of R are also shown. **Fig.12** shows the effects of incidence and R at Mach 0.6 on the separation distribution around the inlet lip.

Fig.13 summarises the predictions for the variation of MFR_{sep} (MFR at flow separation onset) for Mach 0.45 and 0.6 and two Reynolds numbers R_1 and R_2. The symbols indicate MFR values, derived from C_{pmin} peaks, at which separation is well established. The solid lines give a more accurate indication of the onset of separation from curve-fitted C_{pmin} data from experiment. The "dashed" lines show the predicted MFR_{sep} using two possible values of LE radius, corresponding to external (r_{ext}), or internal (r_{int}) surfaces. It is worth remarking that figures such as this, represent a very concise way of condensing a large amount of numerical and experimental data.

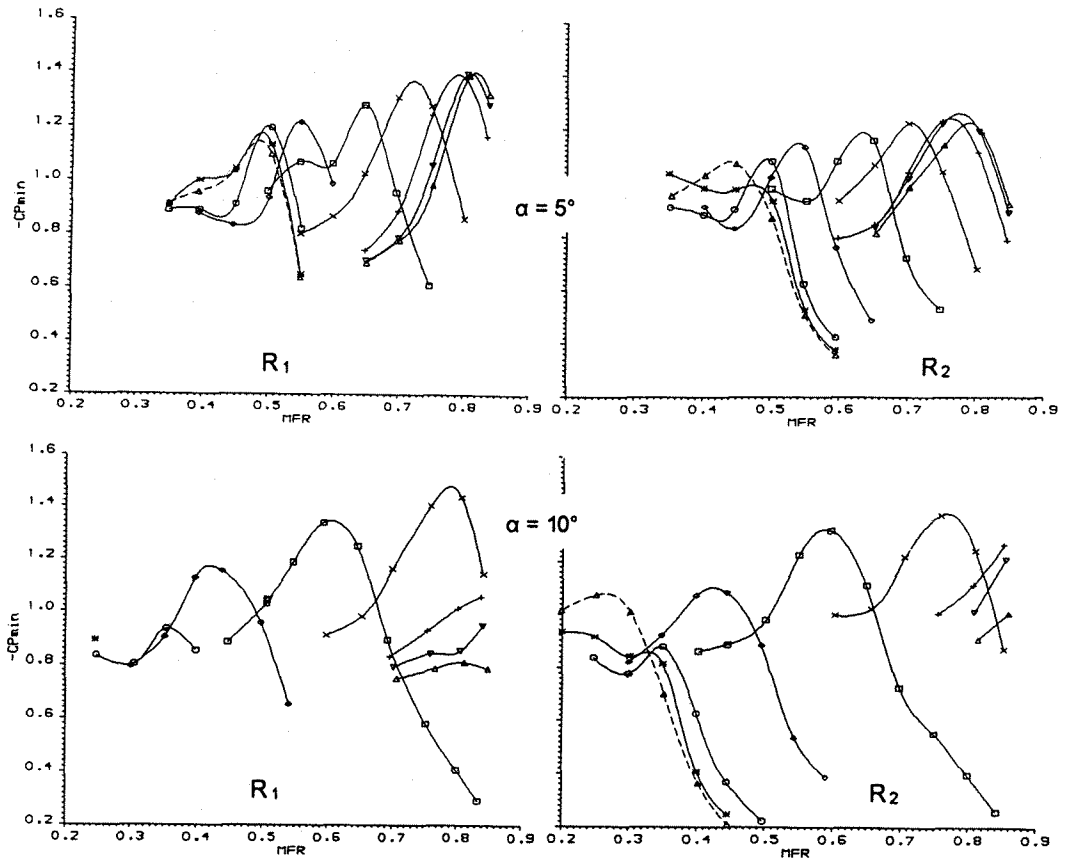

FIG. 12 INLET-A, EXPERIMENTAL C_P TO DISPLAY ONSET OF EXTERNAL FLOW SEPARATION, $\alpha = 5° \& 10°$, Mach 0.6, $R = 1.0 \& 1.7 \times 10^6$

Separation Onset at Mach 0.45

At $\alpha = 5.0°$, flow separation onset predictions are shown, together with results from experiment, for all stations around the inlet. As MFR is reduced, separation initiates from the top of the inlet and there is good correlation between theory and experiment. This good correlation continues around the inlet as MFR is further reduced until separated flow is established over about half the external surface. As MFR is further reduced, external separation from the lower half of the wind tunnel model occurs at a much higher MFR than predicted due to the destabilising effect of the adjacent separated regions.

At $\alpha = 7.5°$ and $10.0°$, flow separation initiates from the top of the inlet at an MFR higher than was achieved in experiment. An ejector would be required to reproduce these higher MFR conditions. The predictions correspond well with the observed separation boundaries in the range $60° < \phi < 90°$ and can therefore be used with confidence to define the onset of flow separation over the upper portion of the inlet, beyond the range achieved in experiment.

Separation Onset at Mach 0.60

Comparisons with experiment show very acceptable correlations. The theory is able to predict in the regions where the experiments could not proceed due to MFR limitations without ejectors e.g. at the top of the cowl at higher α. Predictions at $\alpha = 0.0°$, using a Full Potential solver are also included. These show relatively poor correlation with experiment and this may indicate applicability restriction for such solvers.

3.3. Results on Inlet-B

The tests and analysis on Inlet-B followed similar lines to those on Inlet-A and here we present the correlation between experiment and theory on flow separation onset boundaries.

Fig.14 summarises the predictions for the variation of flow separation onset for Mach 0.45 and 0.6 and two Reynolds numbers R_1 and R_2. Correlation between theory and experiment is as good as for Inlet-A over the full incidence, Mach and R ranges analysed.

The experiment did not fully define the separation boundary around this inlet at any incidence. At $\alpha = 2.5°$ for example, as MFR is reduced, separation has already occurred at the top of the inlet, at an MFR greater than the maximum achieved in experiment. This shows that quite minor changes to the inlet lip profile (Inlet-A to Inlet-B) have significant effects on the inlet performance.

For this inlet, the theory has been able to fully define the separation boundaries at all incidences, Mach number and R values required.

3.4. Other Axi-symmetric Inlets & General Comments

It is worth mentioning that similar encouraging correlations between experiment and theory were obtained for other inlets with different lip shapes, through an incidence range of $\pm 10°$.

It was interesting to observe that in some cases, early separation was detected in experiment compared with the values predicted by theory. Subsequent close inspection of the

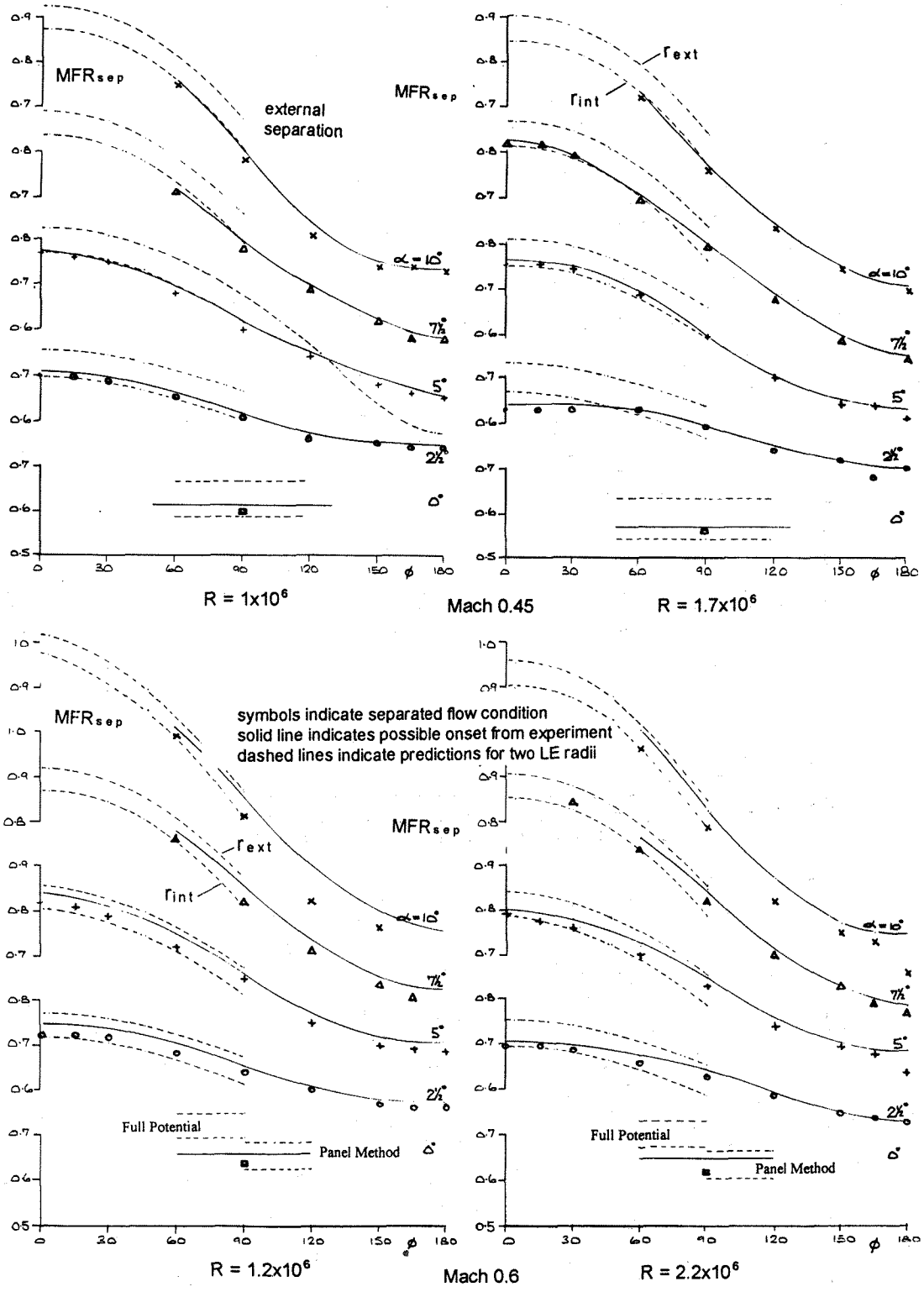

FIG. 13 INLET-A, EXTERNAL SEPARATION BOUNDARIES, THEORY & EXPERIMENT, α = 0.0° to 10.0°, EFFECT OF R, Mach 0.45 & 0.6,

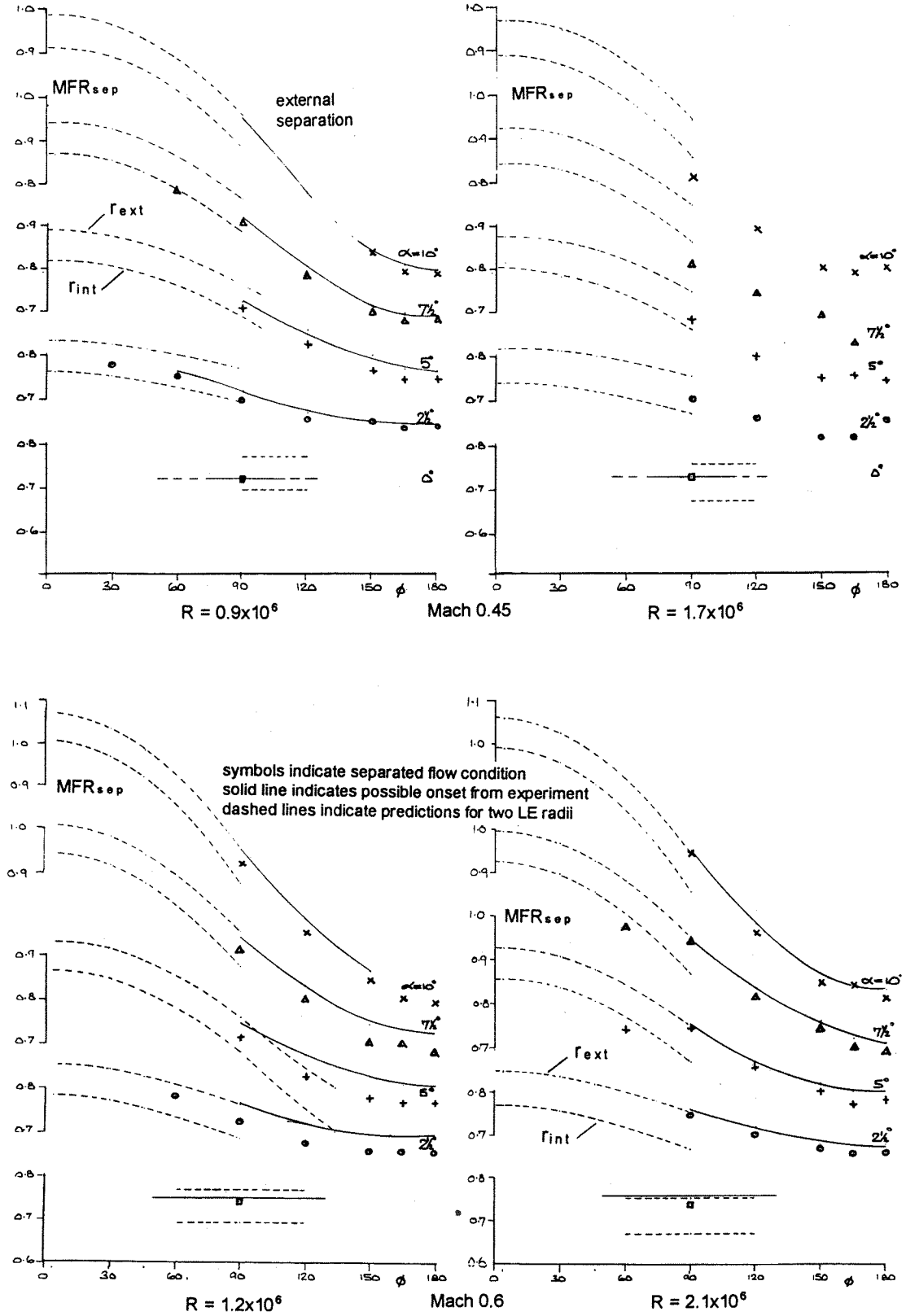

FIG. 14 INLET-B, EXTERNAL SEPARATION BOUNDARIES, THEORY & EXPERIMENT, α = 0.0° to 10.0°, EFFECT OF R, Mach 0.45 & 0.6

wind tunnel models revealed small physical imperfections in the inlet lip surface. This has shown that the theory is capable of highlighting discrepancies in performance resulting from damage or manufacturing defects.

The theory has enabled us to predict separation boundaries in regions (MFR, α, Mach, R) where experiments cannot go without the use of expensive ejector testing.

This encouragement has led us to apply the techniques to more three-dimensional inlet geometries.

4. THREE-DIMENSIONAL (SQUARE CROSS-SECTION) INLETS

Recent work has focussed on relating the axi-symmetric inlet methodology to 3-D square inlets with and without scarf (sweep). **Fig.15** summarises a major effort to determine how the operating capabilities (within the onset of internal and external separations) vary with Reynolds number for 3 different types of inlet, Mach 0.4, $\alpha = 0°$. The three types are: Circular axi-symmetric, Square-prismatic, and Square-scarfed. In general, the inlets had the same streamwise section around the perimeter (NACA-1 series profile externally and ellipse, a/b = 5, internally). The square-scarfed inlet was also studied with different streamwise sections (lip shapes) around the perimeter to improve its performance.

For all three types of inlets, increasing Reynolds number substantially extends the operating range. This aspect is important to know, quantitatively, when extrapolating model scale results to full scale.

At approximately full scale, the operating range of the circular (symmetric) inlet is $\Delta MFR = 0.8$ ($0.5 < MFR < 1.3$). For a rectangular inlet with similar streamwise sections the operating range is also $\Delta MFR = 0.8$ but at $0.6 < MFR < 1.4$.

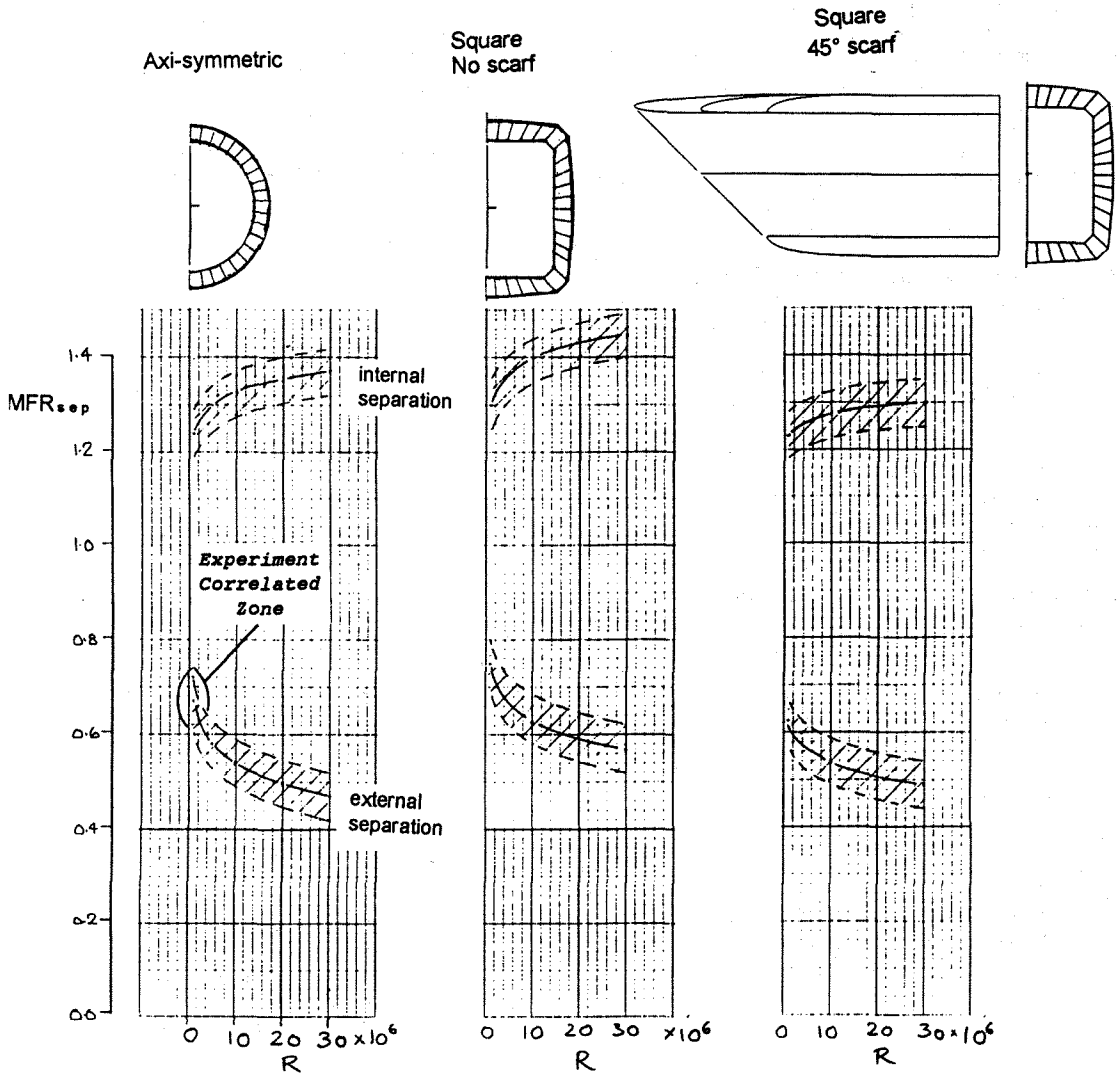

FIG. 15 OPERATING MFR LIMITS OF DIFFERENT INLETS WITH R VARYING

Scarfing the inlet by 45° significantly reduces the operating range to $\Delta MFR = 0.7$, $0.55 < MFR < 1.25$.

This exercise has shown the sensitivity of the design process. Practical configurations can be tackled with the theory and it is currently planned to verify these capabilities with supporting experimental programmes.

5. CONCLUDING REMARKS

Different types of inlets (cowls) are in use. The choice depends upon operational and configuration layout restraints.

For various reasons, combat aircraft require engines to be set close to fuselage centre-line. Further compromises occur because of considerations such as stealth, supersonic capability, transonic and low-speed agility and installation effects, α and ß. The Mass Flow Ratio (MFR) requirements can be challenging particularly in manoeuvring situations.

In civil aircraft, performance, safety, passenger comfort and maintenance considerations lead to "isolated" engine pods or a tail location. Such inlets are characterised by the need for good transonic design (i.e. low distortions) with high MFR capability at low forward velocities (take-off rotation). The incidence effects can be very strong for isolated inlets and although side-slip effects are present, these are not extreme.

For a given inlet, the onset of external or internal flow separation limits the flight envelope. External separation causes a drag increase and internal separations cause distortions at the engine face, leading eventually to compressor surge and possible structural damage. The ability to predict the onset of flow separations is therefore important for their prevention and also to enable more optimum design with shorter ducts.

Conventionally, the inlet design has mainly evolved from an experimental basis (wind tunnel or full-scale); associated high costs and time factors being implicit. The current project scene is more "paced" and emphasises cost and time reductions. This has promoted research towards theoretical / empirical techniques.

This paper has focussed first on the prediction and evaluation methodology for flow separation onset on axi-symmetric circular inlets with and without α effects. The approach has then been extended to 3-D prismatic inlets.

The technique developed addresses the effects of Mach and Reynolds number on inlets in a general way and compared with other approaches available, the capabilities are more design related. Attained thrust principles are used (with and without viscous effects). Thus, increasing Reynolds number at a given Mach number permits a higher proportion of thrust levels to be attained. On the other hand, increasing Mach number at a given Reynolds number, reduces the LE suction level attained. Thin (or sharper) lips reduce the attained thrust levels. Semi-empirical correlations of LE suction attainment factors have been derived from several studies on wings and aerofoils.

Typical results presented for two axi-symmetric inlets at incidence, show extremely encouraging correlation between theory and experiment. Extension of the methodology to 3-D inlets has shown the capability to predict the Mach number and scale effects.

It can be surmised that the work has the potential of providing encouraging cost and time savings in three key areas, initial design, wind tunnel testing and full scale flight testing. New project configurations can be evaluated at an early stage with allowance for scale effects. Configuration layout and flight envelope can all be considered at the design stage.

Optimisation and parametric studies can be carried out using the theory prior to experimental programmes. The theory can also be used to define key areas (M, R, α, ß and MFR) that need to be carefully assessed at the test / evaluation stage.

ACKNOWLEDGEMENTS

The authors have pleasure in acknowledging helpful technical discussions with Mr. S.L. Buckingham (DRA, Bedford) and Mr. P.G. Martin of DRA Bedford, UK. Part of the work was sponsored by the DRA (UK).

Lastly, it should be mentioned that any opinions expressed are those of the authors.

REFERENCES

1. NANGIA, R.K., PALMER, M.E., "Application of Subsonic First-Order Methods for Prediction of Inlet & Nozzle Aerodynamic Interactions with Airframe", AGARD CP, 1991.

2. GOLDSMITH, E.L., & SEDDON, J.E., "Practical Intake Aerodynamic Design", Chap. 3, 4, 7, 8 & 9, Blackwell, 1993.

3. SEDDON, J.E., & GOLDSMITH, E.L., "Intake Aerodynamics", Chap. 4, 9 & 13, Blackwell, 1989.

4. OATES, G.C., "Aircraft Propulsion Systems Technology and Design", Chap. 4 & 6, AIAA, 1989.

5. MURTHY, S.N.B., & PAYNTER, G.C., "Numerical Methods for Engine-Airframe Integration", Chap. 1, 2 & 3, AIAA, 1986.

LIST OF SYMBOLS

a,b	Major and Minor axes of Ellipse
A_0	Capture Area
A_c	Highlight Area
A_{max}	Inlet Maximum External Area
A_t	Throat Area
C_P	Surface Static Pressure Coefficient $(p-p_0)/q$
C_{Pmin}	Lowest Pressure Coefficient, Peak Suction
D, d	Diameter
Hg	Mercury
LE	Leading Edge
M	Mach Number
MFR	Mass Flow Ratio, A_0/A_c
MFR_{sep}	Mass Flow Ratio for Onset of Flow Separation
p	Surface Static Pressure
p_0	Static Pressure
q	Dynamic Pressure $(\frac{1}{2}\rho V^2)$
R	Reynolds number based on Model Diameter
r_{ext}	LE radius, External surface
r_{int}	LE radius, Internal surface
V	Velocity, Freestream
ρ	Air Density
α	Angle of Attack, measured at Inlet axis
ß	Angle of Sideslip
φ	Angular Location around Inlet lip, measured in degrees from the top in a clockwise direction when viewed from rear